Electron and Ion Heating Characteristics during Magnetic Reconnection in the MAST Spherical Tokamak

H. Tanabe,[1,*] T. Yamada,[2] T. Watanabe,[1] K. Gi,[1] K. Kadowaki,[1] M. Inomoto,[1] R. Imazawa,[3] M. Gryaznevich,[4,†] C. Michael,[4] B. Crowley,[4] N. J. Conway,[4] R. Scannell,[4] J. Harrison,[4] I. Fitzgerald,[4] A. Meakins,[4] N. Hawkes,[4] K. G. McClements,[4] T. O'Gorman,[4] C. Z. Cheng,[1,5] Y. Ono[1] and The MAST Team

[1]*Graduate School of Frontier Sciences, University of Tokyo, Tokyo 113-0032, Japan*
[2]*Faculty of Arts and Science, Kyusyu University, Fukuoka 819-0395, Japan*
[3]*Japan Atomic Energy Agency, Ibaraki 311-0193, Japan*
[4]*CCFE, Culham Science Centre, Abingdon, Oxfordshire OX14 3DB, United Kingdom*
[5]*Institute of Space and Plasma Sciences, National Cheng Kung University, Tainan 70101, Taiwan*

(Received 5 May 2015; published 18 November 2015)

Electron and ion heating characteristics during merging reconnection start-up on the MAST spherical tokamak have been revealed in detail using a 130 channel yttrium aluminum garnet (YAG) and a 300 channel Ruby-Thomson scattering system and a new 32 chord ion Doppler tomography diagnostic. Detailed 2D profile measurements of electron and ion temperature together with electron density have been achieved for the first time and it is found that electron temperature forms a highly localized hot spot at the X point and ion temperature globally increases downstream. For the push merging experiment when the guide field is more than 3 times the reconnecting field, a thick layer of a closed flux surface form by the reconnected field sustains the temperature profile for longer than the electron and ion energy relaxation time ~4–10 ms, both characteristic profiles finally forming a triple peak structure at the X point and downstream. An increase in the toroidal guide field results in a more peaked electron temperature profile at the X point, and also produces higher ion temperatures at this point, but the ion temperature profile in the downstream region is unaffected.

DOI: 10.1103/PhysRevLett.115.215004 PACS numbers: 52.35.Vd, 52.55.Fa, 52.72.+v

Magnetic reconnection is a fundamental process that converts the magnetic energy of reconnecting fields to kinetic and thermal energy of plasma through the breaking and topological rearrangement of magnetic field lines [1,2]. Recent satellite observations of solar flares revealed several important signatures of reconnection heating. In the solar flares, hard x-ray spots appear at loop tops of coronas together with another two foot-point spots on the photosphere. The loop-top hot spots are considered to be caused by fast shocks formed in the downstream of reconnection outflow [3]. The two-dimensional (2D) measurements of the Hinode spectrometer documented a significant broadening of Ca linewidth downstream of reconnection [4]. These phenomena strongly suggest direct ion heating by reconnection outflow. On the other hand, the V shape high electron temperature region was found around the X line of reconnection as possible evidence of slow shock structure [5].

However, those heating characteristics of reconnection are still under serious discussion, indicating that direct evidence for the reconnection heating mechanisms should be provided by a proper laboratory experiment. Since 1986, the merging of two toroidal plasmas (flux tubes) has been studied in a number of experiments: TS-3 [6,7], START [8], MRX [9], SSX [10], VTF [11], TS-4 [12], UTST [13,14], and MAST [15]. For those laboratory experiments, evidence of plasma acceleration toward outflow direction was observed as split line-integrated distribution function in 0D [16], 1D, and 2D bidirectional toroidal acceleration during counterhelicity spheromak merging [17,18], and in-plane Mach probe measurement around the X point with and without guide field [19–21]. In the recent TS-3 experiment, with upgrade of diagnostics [22], 2D ion and electron heating characteristics are revealed [23] as bulk heating of ions downstream and localized small electron heating around the X point. The energy inventory has been well investigated in both push merging [24,25] and pull reconnection [26,27]. However, the electron temperature tends to be as low as 15 eV for most of the laboratory experiments due to radiation barrier by low-Z impurities, the presence of invasive probe diagnostics inside the vessel, and convective loss under low guide field conditions [28].

The world's largest merging device MAST [29] (Mega Ampere Spherical Tokamak) achieved remarkable success with those issues. Reconnection heating exceeds ~1 keV at maximum both for ions and electrons [19], duration time exceeds 100 ms without solenoid [30], merging start-up plasma is successfully connected to quasisteady and the H-mode regime [31]. The spatial resolution of Ruby and YAG Thomson scattering diagnostics was recently increased 300 and 130 channels, respectively [32–34]. The limitation of the range of ion temperature profile measurement, normally limited to $r > 0.8$ m due to the innermost impact radius of the neutral beam [35,36], was addressed for these measurements by the temporary repurposing of existing equipment to provide a 32-chord tomographic ion Doppler spectroscopy capability [22,25] on the midplane with a radial

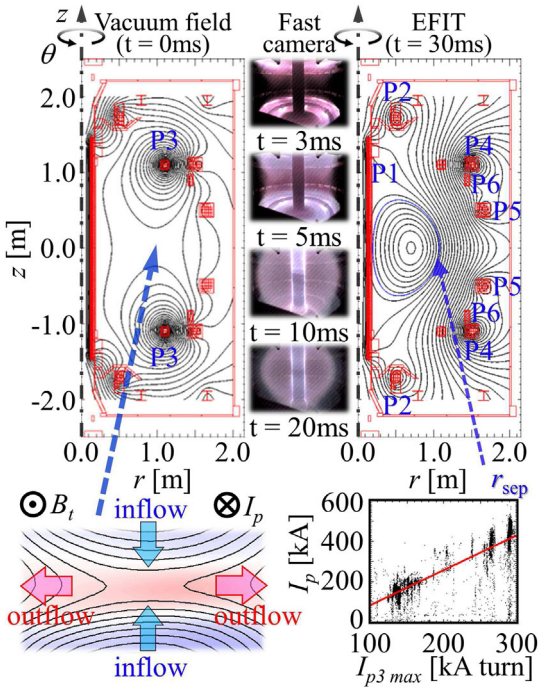

FIG. 1 (color online). The geometry of magnetic reconnection in MAST with flux plots [vacuum field ($t = 0$ ms) and EFIT ($t = 30$ ms)] and fast camera images (mostly D_α emission). Two initial plasma rings are generated around $P3$ coils, move vertically (z direction), and magnetic reconnection is driven at the midplane ($z \sim 0$ m). The achieved maximum plasma current $I_p (\propto B_p)$ linearly increases as a function of the peak current of $P3$ coils $I_{p3\ \mathrm{max}}$.

range spanning the diffusion region. This Letter addresses the first detailed profile measurement of localized electron heating and global ion heating during magnetic reconnection start-up in MAST.

Figure 1 illustrates the geometry of magnetic reconnection and the definition of the coordinates in MAST. In the cylindrical vacuum vessel ($R_{\mathrm{wall}} = 2.0$ m) $P3$ coils generate initial two plasma rings that merge together at the midplane as visualized in the fast camera images [37], and mostly contribute to drive magnetic reconnection in MAST [31,38–41] (plasma current $I_p \propto B_p$ linearly increases as a function of the peak current of $P3$ coils $I_{p3\ \mathrm{max}}$ as shown in Fig. 1, which assembled ~30000 MAST pulses). $P1$ is center solenoid [42], $P2$ generates double null divertor configuration after merging [43], $P4$ and $P5$ control radial equilibrium [30,44], and $P6$ coils control the vertical position [45]. Toroidal field is ~0.3–0.8 T around the diffusion region and the reconnecting field is roughly $B_{\mathrm{rec}} \sim 0.07$–$0.15$ T (based on EFIT reconstruction [46] of the poloidal B_r field after magnetic reconnection at $t = 30$ ms: $B_{\mathrm{rec}} \sim B_p \sim 5.3 \times 10^{-4} I_{p3\,\mathrm{max}}[\mathrm{kA\,turn}] + 2.9 \times 10^{-3}$ T); ion skin depth $c/\omega_{pi} \sim 0.1$ m, ion Larmor radius $\rho_i < 0.01$ m, and ion cyclotron frequency $\omega_{ci} > 10$ Mrad/s. The plasma outer midplane separatrics radius r_{sep} is constantly monitored by a 2048 pixels linear D_α camera ranging $r < 1.8$ m [47]. The 300 channel Ruby and 130 channel Nd:YAG Thomson scattering systems measured electron temperature and density at $z = 0.015$ m with spatial resolution of ~15 mm and $z = -0.015$ m with ~10 mm, respectively, including optical blurring (Ruby-TS (TV Thomson): 302 pixels for wavelength ranging $585.10 < \lambda < 901.15$ nm with instrumental function of ~10 nm (FWHM) but single time frame in each MAST pulse. YAG-TS (filter type): 5 spectral channels for wavelength (central wavelength[nm]/bandwidth[nm]: 755/170, 917/155, 1017.5/45, 1047.5/15, and 1057.7/5.5) and 8 lasers (~30 Hz) for 8 time frames [32–34]). 32 channel ion Doppler tomography diagnostics measures ion temperature profile at midplane ($z \sim 0$ m) with spectral resolution of 0.0078 nm/pixel (512 pixels for wavelength) at 529.05 nm (CVI line) and has viewing chords in $0.25 < r < 1.09$ m [22,25].

As shown in Fig. 2 (top), the P3 ramp down current I_{p3} contributes the formation of initial two plasma rings, magnetic reconnection starts around 5 ms with a large spike of central Mirnov coil signal ($V_{\mathrm{Mirnov}} \propto dB_z/dt$ at $r \sim 0.2$ m, $z \sim 0$ m [48]). The fast camera image in Fig. 1 also shows that two plasma rings move toward midplane around $t = 5$ ms. During the initial spike of V_{Mirnov}, which detects downstream reconnected flux with the microsecond time scale, 130 channel Thomson scattering measurement of n_e and T_e was performed at 8 time frames with the interval of 0.1 ms in the shot 25 740 ($B_{\mathrm{rec}} \sim 0.11$ T and $r_{\mathrm{sep}} \sim 1.0$ m). Before merging ($t = 5.2, 5.3$ ms), electron temperature is as low as ~10 eV and electron density has a peak around the X point. After $t = 5.4$ ms, the built-up density starts to decay and the radial profile of electron density shows clear peak shift, which indicates outflow acceleration toward the radial direction. For the closed flux type reconnection of spherical tokamak (ST) merging, outflow acceleration is damped downstream and forms a double peak profile with shocklike steep density gradient. Electron temperature rapidly increases at $t = 5.5$ ms when the V_{Mirnov} signal reaches its maximum and then the peaked distribution becomes more steep at the X point with a power density of ~0.3 MW/m^3.

Figures 3(a) and 3(b) show 2D electron temperature and density profiles during discharges 21 374–21 380 ($P6$ coils are used to shift the vertical position of Thomson scattering measurement [45]). After 5 ms, outflow ejection continues to increases electron density downstream and forms the current sheetlike structure, while the electron temperature profile forms a characteristic peaked structure at the X point with the scale of 0.02–0.05 m $< c/\omega_{pi}$. In contrast to the no guide field experiment in MRX [27,28] where electron energy gain is quickly transported downstream, the higher toroidal field in MAST strongly inhibits the perpendicular heat conduction if, as expected, this scales as of $1/B_t^2$ and the established profile is sustained in millisecond time scale. At $t = 10$ ms, cross validation with the 300 channel Ruby

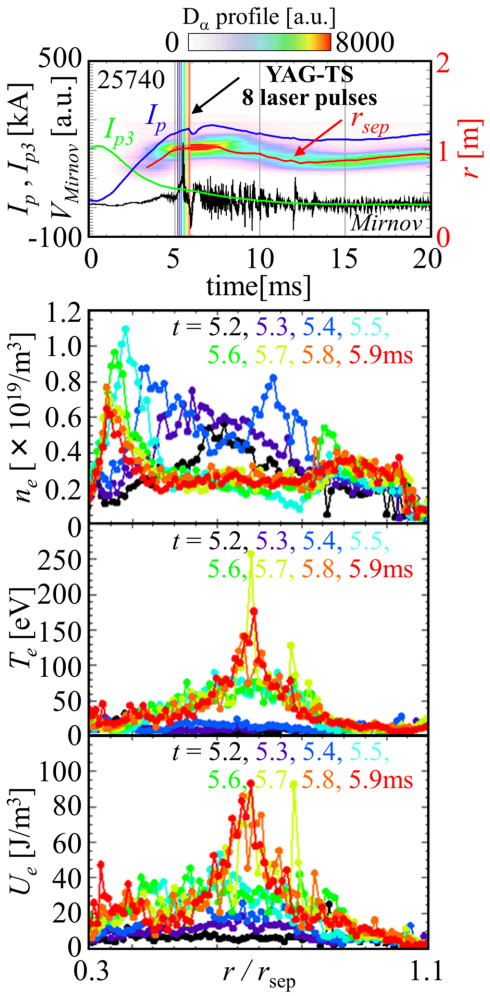

FIG. 2 (color online). Time resolved Thomson scattering measurement of electron density and temperature profile from 5.2 ms with the interval of 0.1 ms with the reference information of the time scale of fast reconnection events in MAST. During the initial spike of the central Mirnov coil, magnetic reconnection starts and the buildup electron density at the X point was ejected towards downstream, while electrons are heated around the X point from ~10 to ~200 eV within 1 ms.

Thomson scattering measurement is also performed and successfully reproduces the highly localized hot spot at the X point. In addition, the electron temperature profile also forms the characteristic high T_e area downstream. It is located around the high density region where reconnection outflow should dissipate, suggesting the effect of energy relaxation between electrons and ions to equilibrate both temperatures. Figure 3(c) illustrates the 2D ion temperature profile in pulses 30 366–30 368, 30 376–30 377 ($B_{\rm rec} \sim 0.08$ T). Ions are mostly heated in the downstream region of outflow acceleration inside the current sheet width ($c/\omega_{pi} \sim 0.1$ m) and around the stagnation point mostly by viscosity dissipation [9,27] and shocklike compressional damping of the outflow jet [19,23], as in the two fluid simulation which includes such fundamental collisional viscous dissipation

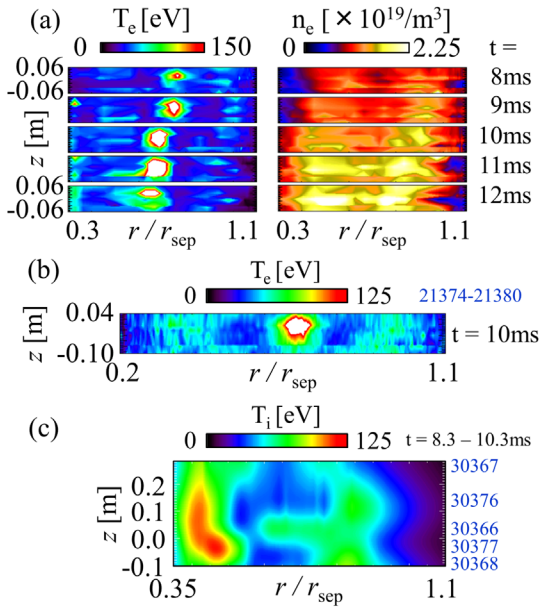

FIG. 3 (color online). 2D Thomson scattering measurement of electron temperature and density profile at $t = 8$, 9, 10, 11, and 12 ms around the X point (a), 300 channel fine T_e profile using Ruby Thomson scattering measurement (b) and 2D ion temperature profile using 32 chords ion Doppler Tomography diagnostics (c).

[40,41]. For the high guide field reconnection experiment in MAST, the ratio of collisional thermal diffusivities $\chi^i_\parallel/\chi^i_\perp \sim 2(\omega_{ci}\tau_{ii})^2 \gg 10$ is much higher than that of other laboratory experiments ($\chi^i_\parallel/\chi^i_\perp \sim 1$ for the null-helicity operation in MRX [49]). Thus, toroidal configuration also contributes the characteristic temperature profile, outflow heating downstream forms a ring structure of the closed flux surface [40,41] and enhances the local energy relaxation between ions and electrons in the millisecond time scale of τ^E_{ei}, and, finally, contributes the electron heating in the outflow region.

Figure 4 shows time evolution of more detailed 1D profiles of electron and ion temperature ($B_{\rm rec} \sim 0.08$ T) in the comparable time scale of $\tau^E_{ei} \sim 4$–10 ms. Before

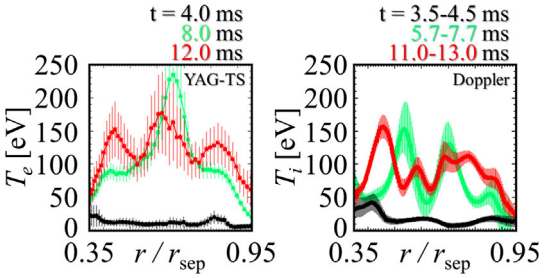

FIG. 4 (color online). 1D radial profile of T_e and T_i at the midplane [CIII (464.7 nm) line was used in the frame of $t = 3.5$–4.5 ms]. Electrons are mostly heated at the X point and ions in the outflow region. Both profiles finally form triple peaks through the energy transfer of ions and electrons with the delay of τ^E_{ei}.

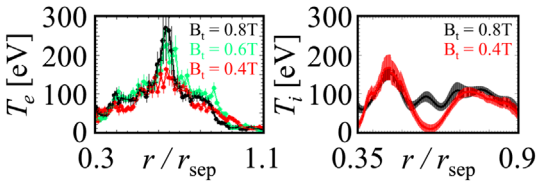

FIG. 5 (color online). Effect of the guide field for the formation of the characteristic temperature distribution. The structure of the peaked T_e profile becomes more steep with better confinement under high guide field conditions and also contributes ion heating at the X point by $T_i - T_e$ energy transfer, while the downstream ion temperature does not change.

merging, both temperatures are as low as ~10 eV. During magnetic reconnection, electrons are mostly heated at the X point, while the ion temperature profile forms double peaks in the outflow region. The characteristic different temperature distribution for both are relaxed to each other with the millisecond time scale by the collisional coupling between ions and electrons; finally, both profiles form a triple peak structure at $t \sim 12$ ms.

Figure 5 shows the effect of guide field for electron and ion heating with $B_{\mathrm{rec}} \sim 0.08$ T. The localized X point electron temperature profile becomes more steep under high guide field conditions probably because the higher guide field strongly inhibits cross-field thermal transport scaling as $1/B_t^2$, so that the electrons remain in the region of high toroidal electric field for longer, or the enhancement of steep sheet current profile for smaller amplitude of meandering motions by higher guide field [50]. Such characteristic distribution also affects the ion temperature profile around the X point. Because the perpendicular heat conduction of ions is expected to scale as $1/B_t^2$, ions also gain energy around the X point under higher guide field conditions, finally forming a triple peak structure. However, bulk ion heating downstream does not change as demonstrated in the push ST merging experiment with intermittent plasmoid ejection in TS-3 [51] and PIC simulation [52]. For the operation range of ultrahigh guide field conditions $B_t >$ 0.3 T and $B_t/B_{\mathrm{rec}} > 3$, outflow dissipation by viscosity damping is suppressed [53,54]; however, the improved confinement by higher guide field assists the confinement time of ions at downstream in a local closed flux surface, finally damps outflow and the dissipated flow energy heat ions downstream as in two fluid simulation [41].

In summary, electron and ion heating characteristics during magnetic reconnection under high guide field conditions in MAST has been investigated using noninvasive and sub-cm ultrafine optical diagnostics. 2D detailed imaging measurement of temperature profile around the diffusion region has been achieved for the first time and it was found that high guide field reconnection heats electrons locally at the X point and ions globally downstream. The 2D profile of electron temperature forms highly localized peaked structure at the X point with the characteristic scale length of 0.02–0.05 m $< c/\omega_{pi}$, while ion temperature increases inside the acceleration channel of reconnection outflow with the width of $c/\omega_{pi} \sim 0.1$ m and the downstream where the reconnected field forms a thick layer of closed flux surface. The $T_i - T_e$ energy relaxation process, which is too slow for a short pulse laboratory experiment ($\tau_{\mathrm{duration}} \ll \tau_{ei}^E$) and too fast ($\tau_{\mathrm{event}} \gg \tau_{ei}^E$) for astrophysical plasma, also affects both temperature profiles in the middle time scale experiment in MAST. With the delay of τ_{ei}^E after the rapid temperature increase of electrons at the X point and ions downstream, the equilibration process to form a triple peak structure for both profiles by $T_i - T_e$ relaxation was observed for the first time and contributes to connect the gap of time scale between typical laboratory experiments and astrophysical events. The toroidal guide field mostly contributes to the formation of the peaked electron temperature profile at the X point and not to bulk ion heating downstream under the ultrahigh guide field condition in MAST. Although the absence of direct magnetic probe measurement limits the possible discussion of the formation mechanism of the characteristic heating profile, it should be noted that the ultrafine noninvasive optical diagnostics in MAST successfully reveal the existence of a highly peaked electron temperature profile at the X point without breaking the structure whose scale is comparable to typical invasive probe diagnostics. In addition, the achieved bulk (downstream) electron temperature reaches comparable order to ion temperature after the delay of τ_{ei}^E and succeeded in pioneering the application of reconnection heating for CS-less start-up of spherical tokamak even in the ultrahigh guide field regime ($B_t > 0.3$ T), which is preferable for better confinement in practical operation.

This work was supported by Grant-in-Aid for Scientific Research 22246119, 22656208, 25820434, 15H05750, and 15K20921, JSPS Core-to-Core program 22001, JSPS institutional Program for Young Researcher Overseas Visits, and NIFS Collaboration Research Programs (NIFS11KNWS001, NIFSKLEH024, and NIFS11KUTR060). This work was also partly funded by the RCUK Energy Programme under Grant No. EP/I501045 and the European Communities. The views and opinions expressed herein do not necessarily reflect those of the European Commission. We acknowledge Adam Stanier and Alan Sykes for useful discussion and Samuli Saarelma, Ian Chapman, and Brian Lloyd for managing the campaign shots for the reconnection studies.

*tanabe@k.u-tokyo.ac.jp
†Present address: Tokamak Energy, Culham Innovation Centre, Abingdon, Oxfordshire, OX14 3DB, United Kingdom.

[1] M. Yamada, R. Kulsrud, and H. Ji, Rev. Mod. Phys. **82**, 603 (2010).
[2] E. G. Zweibel and M. Yamada, Annu. Rev. Astron. Astrophys. **47**, 291 (2009).
[3] S. Masuda, T. Kosugi, H. Hara, S. Tsuneta, and Y. Ogawara, Nature (London) **371**, 495 (1994).

[4] H. Hara, T. Watanabe, Louise K. Harra, J. Leonard Culhane, and P. R. Young, Astrophys. J. **741**, 107 (2011).
[5] T. Shimizu, S. Tsuneta, L. W. Acton, J. R. Lemen, Y. Ogawara, and Y. Uchida, Astrophys. J. **422**, 906 (1994).
[6] Y. Ono *et al.*, *Proceedings of the 1986 IEEE International Conference on Plasma Science, Saskatoon, Canada, 1986* (IEEE, New York, 1986), p. 77.
[7] Y. Ono, A. Morita, M. Katsurai, and M. Yamada, Phys. Fluids B **5**, 3691 (1993).
[8] M. Gryaznevich *et al.*, Phys. Rev. Lett. **80**, 3972 (1998).
[9] M. Yamada, H. Ji, S. Hsu, T. Carter, R. Kulsrud, N. Bretz, F. Jobes, Y. Ono, and F. Perkins, Phys. Plasmas **4**, 1936 (1997).
[10] M. R. Brown, Phys. Plasmas **6**, 1717 (1999).
[11] J. Egedal, A. Fasoli, M. Porkolab, and D. Tarkowski, Rev. Sci. Instrum. **71**, 3351 (2000).
[12] Y. Ono, T. Kimura, E. Kawamori, Y. Murata, S. Miyazaki, Y. Ueda, M. Inomoto, A. L. Balandin, and M. Katsurai, Nucl. Fusion **43**, 789 (2003).
[13] T. Yamada *et al.*, Plasma Fusion Res. **5**, S2100 (2010).
[14] M. Inomoto *et al.*, Nucl. Fusion **55**, 033013 (2015).
[15] M. Gryaznevich *et al.*, Phys. Plasmas **10**, 1803 (2003).
[16] T. Gray, V. S. Lukin, M. R. Brown, and C. D. Cothran, Phys. Plasmas **17**, 102106 (2010).
[17] Y. Ono, M. Yamada, T. Akao, T. Tajima, and R. Matsumoto, Phys. Rev. Lett. **76**, 3328 (1996).
[18] H. Tanabe, H. Oka, M. Annoura, A Kuwahata, K. Kadowaki, Y. Kaminou, S. You, A. Balandin, M. Inomoto, and Y. Ono, Plasma Fusion Res. **8**, 2405088 (2013).
[19] Y. Ono *et al.*, Plasma Phys. Controlled Fusion **54**, 124039 (2012).
[20] J. Yoo, M. Yamada, H. Ji, J. Jara-Almonte, C. E. Myers, and L. J. Chen, Phys. Rev. Lett. **113**, 095002 (2014).
[21] J. Yoo, M. Yamada, H. Ji, and C. E. Myers, Phys. Rev. Lett. **110**, 215007 (2013).
[22] H. Tanabe, A. Kuwahata, H. Oka, M. Annoura, H. Koike, K. Nishida, S. You, Y. Narushima, A. Balandin, M. Inomoto, and Y. Ono, Nucl. Fusion **53**, 093027 (2013).
[23] Y. Ono, H. Tanabe, Y. Hayashi, T. Ii, Y. Narushima, T. Yamada, M. Inomoto, and C. Z. Cheng, Phys. Rev. Lett. **107**, 185001 (2011).
[24] Y. Ono, M. Inomoto, T. Okazaki, and Y. Ueda, Phys. Plasmas **4**, 1953 (1997).
[25] Y. Ono, H. Tanabe, T. Yamada, K. Gi, T. Watanabe, T. Ii, M. Gryaznevich, R. Scannell, N. Conway, B. Crowley, and C. Michael, Phys. Plasmas **22**, 055708 (2015).
[26] S. C. Hsu, G. Fiksel, T. A. Carter, H. Ji, R. M. Kulsrud, and M. Yamada, Phys. Rev. Lett. **84**, 3859 (2000).
[27] M. Yamada, J. Yoo, J. Jara-Almonte, H. Ji, R. M. Kulsrud, and C. E. Myers, Nat. Commun. **5**, 4774 (2014).
[28] J. Yoo, M. Yamada, H. Ji, J. Jara-Almonte, and C. E. Meyers, Phys. Plasmas **21**, 055706 (2014).
[29] B. Lloyd *et al.*, Nucl. Fusion **51**, 094013 (2011).
[30] M. Gryaznevich, IEEJ Trans. Fund. Mater. **125**, 881 (2005).
[31] A. Sykes *et al.*, Nucl. Fusion **41**, 10 (2001).
[32] M. J. Walsh, E. R. Arends, P. G. Carolan, M. R. Dunstan, M. J. Forrest, S. K. Nielsen, and R. O'Gorman, Rev. Sci. Instrum. **74**, 1663 (2003).
[33] E. R. Arends, Ph.D. thesis, Eindhoben University of Technology, 2003 (https://www.differ.nl/node/1512).
[34] R. Scannell, M. J. Walsh, M. R. Dunstan, J. Figueiredo, G. Naylor, T. O'Gorman, S. Shibaev, K. J. Gibson, and H. Wilson, Rev. Sci. Instrum. **81**, 10D520 (2010).
[35] N. J. Conway, P. G. Carolan, J. McCone, M. J. Walsh, and M. Wisse, Rev. Sci. Instrum. **77**, 10F131 (2006).
[36] A. Sykes *et al.*, in *Proceedings of the 32nd EPS Conference on Plasma Phys., Tarragona, 2005* (EPS, Tarragona, 2005), P 4.112.
[37] A. Kirk *et al.*, Plasma Phys. Controlled Fusion **48**, B433 (2006).
[38] A. Stanier, P. Browning, M. Gordovskyy, K. G. McClements, M. P. Gryaznevich, and V. S. Lukin, Phys. Plasmas **20**, 122302 (2013).
[39] P. K. Browning, A. Stanier, G. Ashworth, K. G. McClements, and V. S. Lukin, Plasma Phys. Controlled Fusion **56**, 064009 (2014).
[40] A. Stanier, Ph.D. thesis, The University of Manchester, 2013, p. 203, https://www.escholar.manchester.ac.uk/ jrul/item/?pid=uk-ac-man-scw:211308.
[41] P. K. Browning, S. Cardnell, M. Evans, F. Arese Lucini, V. S. Lukin, K. G. McClements, and A. Stanier, arXiv:1507.07432 [Plasma Phys. Controlled Fusion (to be published)].
[42] M. Cox and MAST Team, Fusion Eng. Des. **46**, 397 (1999).
[43] B. Lloyd *et al.*, Nucl. Fusion **43**, 1665 (2003).
[44] I. T. Chapman *et al.*, Nucl. Fusion **55**, 104008 (2015).
[45] G. Cunningham, Fusion Eng. Des. **88**, 3238 (2013).
[46] L. L. Lao, H. St. John, R. D. Stambaugh, A. G. Kellman, and W. W. Pfeiffer, Nucl. Fusion **25**, 1611 (1985).
[47] J. Storrs, J. Dowling, G. Counsell, and G. McArdle, Fusion Eng. Des. **81**, 1841 (2006).
[48] T. Edlington, R. Martin, and T. Pinfold, Rev. Sci. Instrum. **72**, 421 (2001).
[49] A. Kuritsyn, Ph.D. thesis, Princeton University, 2005, p. 125.
[50] R. Horiuchi, S. Usami, and H. Ohtani, Plasma Fusion Res. **9**, 1401092 (2014).
[51] Y. Ono, Y. Hayashi, T. Ii, H. Tanabe, S. Ito, A. Kuwahata, T. Ito, Y. Kamino, T. Yamada, M. Inomoto, and (TS-Group), Phys. Plasmas, **18**, 111213 (2011).
[52] S. Inoue, Y. Ono, H. Tanabe, R. Horiuchi, and C. Z. Cheng, Nucl. Fusion, **55**, 083014 (2015).
[53] S. I. Braginskii, in *Reviews of Plasma Physics*, edited by M. A. Leontovich (Consultants Bureau, New York, 1965), Vol. 1, p. 205.
[54] Z. Yoshida, Nucl. Fusion **31**, 386 (1991).